5 ZEPLIN and LUX

Behind the potential of LZ lie a highly developed and well-understood technology and a team with a long track record in dark-matter searches with LXe. This section describes the ZEPLIN and LUX programs, with emphasis on the technical developments relevant to LZ. The confluence of these two programs led directly to LZ — although we draw also from significant experience from XENON10, CDMS, CRESST, Edelweiss, EXO-200, Daya Bay, and other rare-event searches, which have engaged many LZ collaborators in the past.

5.1 The ZEPLIN Program at Boulby

The Xe-based ZEPLIN program at the Boulby mine (UK) dates back to the 1990s [1-3]. It coalesced around the UK Dark Matter Collaboration (UKDMC), which had been exploring the viability of various WIMP search technologies for a few years. The first dark-matter results were published from a sodium iodide crystal [4], leading subsequently to the NAIAD (NaI Advanced Detector) experiment, which operated until 2003 [5,6]. The ZEPLIN and DRIFT (Directional Recoil Identification From Tracks) programs followed, the latter developing gaseous TPC detectors to measure recoil directionality [7,8].

ZEPLIN-I exploited pulse-shape discrimination (PSD) in an LXe scintillation detector, publishing final results in 2005 [9]. It featured at its core a PTFE-lined chamber containing a 5 kg LXe target viewed by three 3-inch photomultipliers (PMTs) coupled to quartz windows, as shown in Figure 5.1.1 (left). This was followed by the first double-phase Xe TPCs, ZEPLIN-II and ZEPLIN-III, in which the ionization response was also detected via electroluminescence developed in a thin layer of vapor above the liquid [10]. Besides affording much better discrimination than the simple PSD technique exploited in ZEPLIN-I, this second signature allows precise 3-D reconstruction of the interaction site and a very low NR energy threshold, being sensitive down to individual electrons emitted from the liquid [11-13]. ZEPLIN-II, shown in Figure 5.1.1 (center and right), became the first double-phase system to operate underground, completing in 2007 [14,15]. It featured a deep, high-reflectance PTFE chamber containing 31 kg of LXe with readout from seven PMTs in the gas phase. ZEPLIN-III [16] concluded the Boulby program, with science runs in 2008 [17,18] and, following an upgrade phase, in 2010-11 [19]; it utilized 31 PMTs immersed in the liquid, viewing a thin disc geometry of 12.5 kg of LXe at high electric field.

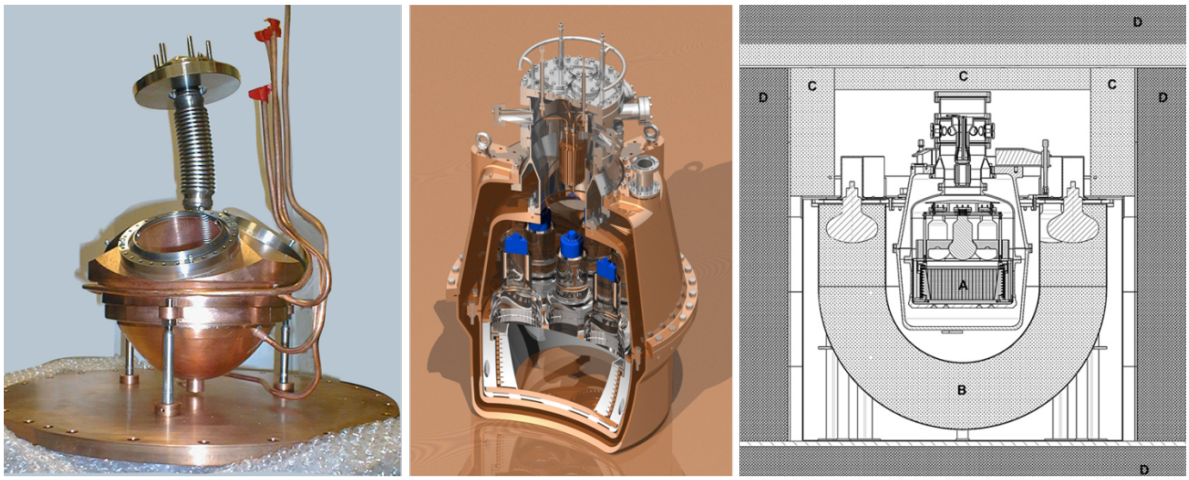

Figure 5.1.1. Left: Liquid xenon chamber of the ZEPLIN-I detector as built; three quartz windows permitted viewing of the 5 kg WIMP target by photomultipliers operating warm. Center: Schematic representation of the ZEPLIN-II detector, where the PTFE-lined chamber is viewed by seven PMTs in the gas phase. Right: Both systems were operated within a liquid scintillator veto detector (B), shielded by Gd-loaded polyethylene (C) and lead (D).

A main aim of the UK program was to evaluate the distinct technical solutions adopted in both detectors, with a view to building a tonne-scale experiment, ZEPLIN-MAX. However, with the timely development of LUX, a merger between the ZEPLIN-III and LUX teams became the sensible continuation of the UK program and a memorandum of understanding (MOU) was signed in 2008, leading to LZ.

5.1.1 ZEPLIN-III

The ZEPLIN-III experiment achieved the best WIMP sensitivity of the Boulby program and demonstrated important features that now inform the design and exploitation of double-phase Xe experiments. The instrument construction is described in [16]; the main components of the experiment are illustrated in Figure 5.1.1.1. Its most innovative features were the thin disc geometry, to permit application of a strong electric field to the target, and the immersion of the PMTs directly in the cold liquid phase, for improved light collection. Most elements were built from high-purity copper to minimize background. The outer cryostat vessel enclosed two chambers; the lower one contained the LN_2 coolant, which boiled off through a heat exchanger attached to the Xe vessel above it. The latter housed a 12.5-kg LXe WIMP target, with the immersed PMTs viewing upward to maximize detection efficiency for the primary scintillation. The active volume was formed by an anode disc 39.2 cm in diameter and a cathode wire grid located 4 cm below it, and a few mm above the PMT array.

Contrary to ZEPLIN-II, where a wire-grid just below the liquid surface helped with cross-phase emission, in ZEPLIN-III the planar geometry allowed application of a strong field to the whole liquid phase with only two electrodes, thus enhancing the efficiency for charge extraction from the particle tracks. Typical

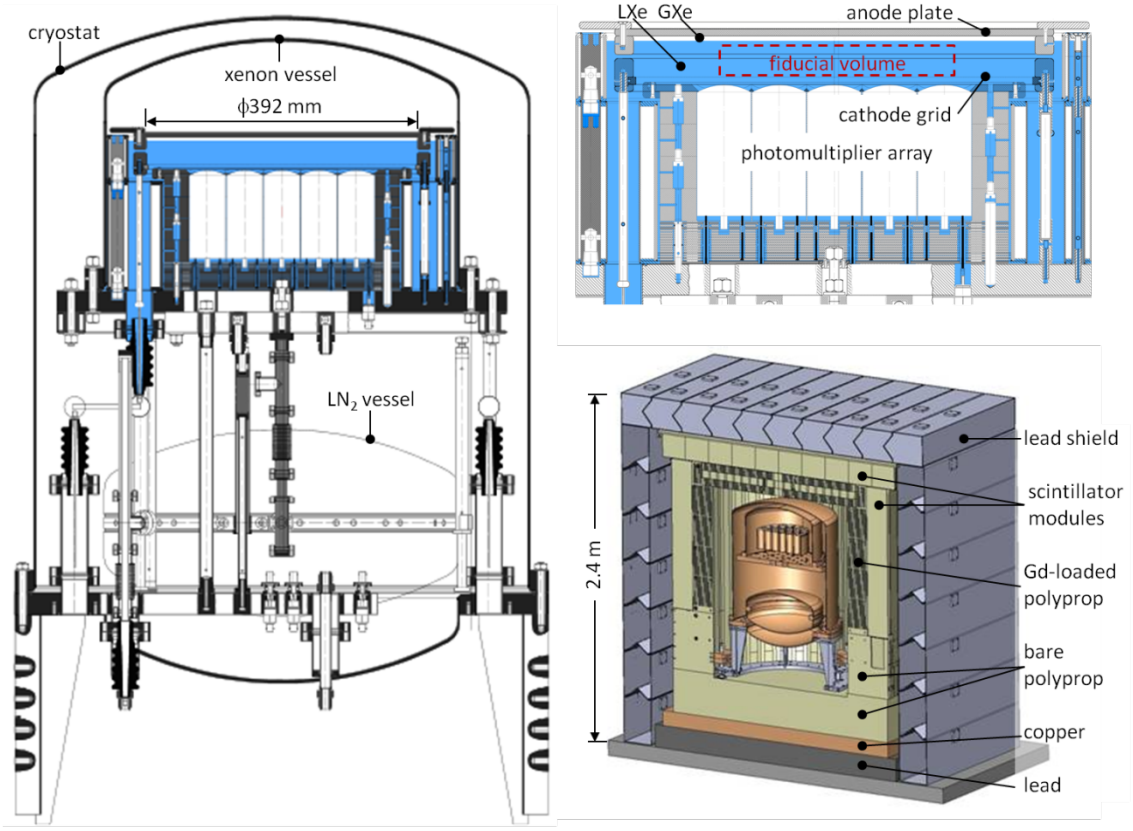

Figure 5.1.1.1. Schematic drawings of the ZEPLIN-III experiment. Left: The WIMP target, with LXe in blue. Top right: The double-phase chamber, with an approximate fiducial volume indicated in dashed red. Lower right: The fully shielded configuration at Boulby (including a plastic veto instrument surrounding the WIMP target) [20,16,21].

operating fields were 3–4 kV/cm in the liquid and approximately twice as strong in the gas [17,19]. A second wire-grid just above the PMTs isolated their input optics from the external field. Only Xe-friendly, low-outgassing materials were used within this chamber, in particular avoiding any plastics, in order to maintain sufficient electron lifetime in the liquid without continuous purification. This was indeed achieved, with the lifetime even improving steadily over one year of operation in the closed system [22].

In the first science run, custom-made PMTs (ETEL D730Q/9829QA) were used; these had bialkali photocathodes with metal fingers deposited on quartz windows under the photocathode for low-temperature operation. The average (cold) quantum efficiency for Xe light was 30% [23]. For the second science run, those PMTs were replaced with a pin-by-pin compatible model with 40 times lower radioactivity (35 mBq per unit in gamma activity), lowering the overall electromagnetic background of the experiment to 750 mdru at low energy [24]. Unfortunately, their optical performance was much poorer, with only 26% mean quantum efficiency and very large gain dispersion [22]. For this reason, ETEL PMTs are not considered as a viable option for LZ.

Between the two science runs, an anticoincidence "veto" instrument was fitted around the WIMP target (shown in Figure 5.1.1.1), replacing some of the hydrocarbon shielding. This veto detector counted 52 plastic scintillator modules with independent PMT readout, arranged into barrel and roof sections, surrounding a Gd-loaded polypropylene structure tailored for neutron moderation and efficient radiative capture (vetoing ~60% of neutrons) [21,25,19]. Events tagged promptly during science running — exclusively gamma rays, vetoed with 28% efficiency [19] — provided access to a low-energy data set that could be used without compromising a blind analysis. The veto system also allowed the independent measurement of muon-induced neutron production from the lead shield around the experiment [26]. Accurate position reconstruction of particle interactions in three dimensions allows a fiducial volume to be defined very precisely, well away from any surfaces and avoiding outer regions with non-uniform electric field and light collection. A typical gamma-ray event is shown in Figure 5.1.1.2 (left). The depth coordinate was obtained with precision of a few tens of μm from the drift time of the ionization charge.

The horizontal coordinates were reconstructed from S2 signals from all PMTs; a spatial resolution of 1.6 mm (FWHM) was achieved for 122 keV gamma rays [27], using the novel Mercury algorithm now applied also to LUX. Other significant analysis algorithms were developed by the project, namely

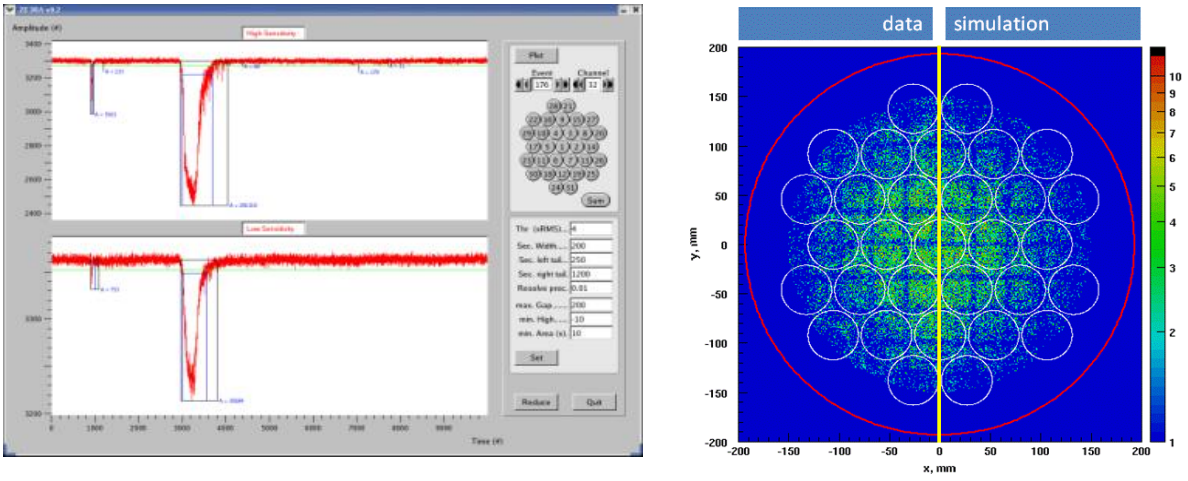

Figure 5.1.1.2. Left: Gamma ray interaction in ZEPLIN-III, showing a fast scintillation signal (S1) followed by a large electroluminescence pulse (S2); a high-sensitivity channel is displayed in the upper panel, and a lower gain channel in the lower one. Right: Calibration and Monte Carlo data for ^{57}Co gamma rays incident from above the detector. The grid-like structure arises from a copper absorber placed directly on top of the solid anode plate; the simulation assumes perfect position resolution; the data are reconstructed with the Mercury algorithm [27].

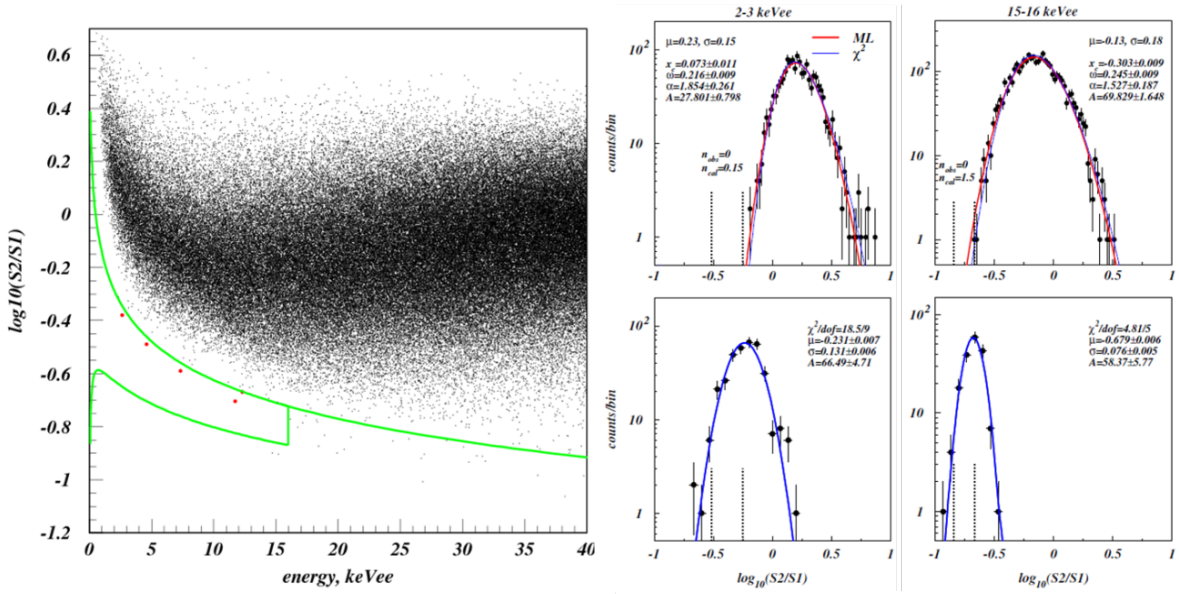

Figure 5.1.1.3. Left: First (83-day) WIMP-search run of ZEPLIN-III; the average electron/nuclear recoil discrimination in the 2–16 keVee acceptance region was 99.99% for 50% NR acceptance. Right: Fitting of ER band for lowest and highest 1-keVee wide bins to a skew-Gaussian function (upper panel) and of the NR band, obtained with an Am-Be neutron source, with a Gaussian function [17].

ZE3RA, a full data-reduction and display software tool [28], and a new technique to calibrate photomultiplier arrays under exact data conditions [29].

A fiducial volume containing 6.5 kg of LXe was defined for the 83-day first run of ZEPLIN-III [17], decreasing to 5.1 kg for the 319-day second run, owing to the poorer PMT performance. The NR threshold for WIMP searches was ~7 keV in both runs [30], determined by the scintillation yield of the chamber (5.0 phe/keV for ^{57}Co gamma rays at zero electric field); the ionization threshold was five S2 electrons. A rejection efficiency of 99.99% (for ER leakage past the NR median) was achieved at WIMP-search energies in the first run, which remains the best reported for double-phase Xe. This is shown in Figure 5.1.1.3, where the S2/S1 discrimination parameter is plotted for first WIMP search; histograms of this parameter for the nuclear and electron recoil populations are also shown.

In both runs, a handful of events were observed within the signal-acceptance region, consistent with background expectations in both cases. The combined result excluded a WIMP-nucleon scalar cross section above 3.9×10^{-44} cm^2 at 90% CL for a 50 GeV/c^2 WIMP mass [19].

The early parallel development of ZEPLIN-II and ZEPLIN-III contributed to the success of double-phase Xe, pursued subsequently by the XENON program and now by LUX. Different approaches were deliberately explored for most subsystems. At the core of the detectors, different designs were implemented for light collection (PMTs in the gas or in the liquid, high-reflectance PTFE chamber or shallow, disc-like target, respectively), electric field in the drift region (1 kV/cm and 4 kV/cm), design of the electroluminescence region (3-electrode and 2-electrode chambers), readout granularity, and position resolution (seven 3-inch or 31 2-inch PMTs). Other subsystems were likewise dissimilar: liquefaction method and thermal control (LXe "raining" from a "cryocooler" cold-head above the target or internal LN_2 heat exchanger at the bottom plate), the approach to LXe purity (external recirculation or clean chamber construction), the powering of the PMTs (internal voltage divider bases versus common "dynode plates" fed externally), general construction materials (faster construction using cast metal or machined ultrapure copper). This invaluable experience propagated to the design of other systems around the world.

5.2 LUX: The Large Underground Xenon Experiment

The LUX experiment [31] is the most recent two-phase Xe dark-matter detector to begin operations, and in its first result [32] it has achieved world-leading WIMP sensitivity for WIMP masses above 6 GeV/c^2. The basic technology follows on more than a decade of effort from the ZEPLIN and XENON programs.

LUX has introduced a number of important innovations that will be important for LZ, including a low-radioactivity titanium cryostat, nitrogen thermosyphons, high-flow Xe purification, two-phase Xe heat exchangers, internal calibration with gaseous sources of ^{83m}Kr and ^{3}H, and nuclear recoil calibration using multiple scatters of monoenergetic neutrons. A schematic of LUX is shown in Figure 5.2.1.

The LUX cryostat vessels are fabricated from Ti with very low levels of radioactivity [33], rivaling even copper, which is highly radiopure but has inferior mechanical properties and is much denser. The high strength-to-weight ratio and low Z of Ti also give it low stopping power for gamma rays, which will enhance the efficiency of the outer detector system in LZ.

The two-phase TPC technique requires precise control of the thermodynamic environment, and this was achieved in LUX through the development of an innovative system of nitrogen thermosyphons. These feature precise, automated control of cooling up to hundreds of kW, plus simple and reliable remote operation. Among other things, this system has allowed highly controlled initial cooling of the system [34], which is necessary to avoid warping of the large plastic structures of the TPC — also a concern in LZ. A related development is the fluid-circulation system that allows rapid circulation of LXe through an external gas-phase getter at flows exceeding 25 standard liters per minute, while maintaining a stable liquid surface through the use of a weir. Using an innovative two-phase heat exchanger system [35], it obtained very efficient heat transfer between evaporating and condensing Xe streams, and thus negligible overall heat load on the detector. Xe purification was greatly aided by the use of an innovative gas trapping and mass spectrometry system [36,37] that is sensitive to impurities at the sub-ppb concentration needed for good electron transport and light collection. This qualitatively new level of diagnostic capability allowed us to monitor various portions of the gas system and detector and efficiently track down any sources of contaminant. These systems were demonstrated during LUX's first science run, where cooldown was achieved in only nine days, and sufficient purity in terms of electron drift lifetime to begin science operations was achieved only ~1 month after filling with LXe (see Figure 5.2.2). Afterward, we achieved stable operation of the detector with mostly unattended operation over a several-

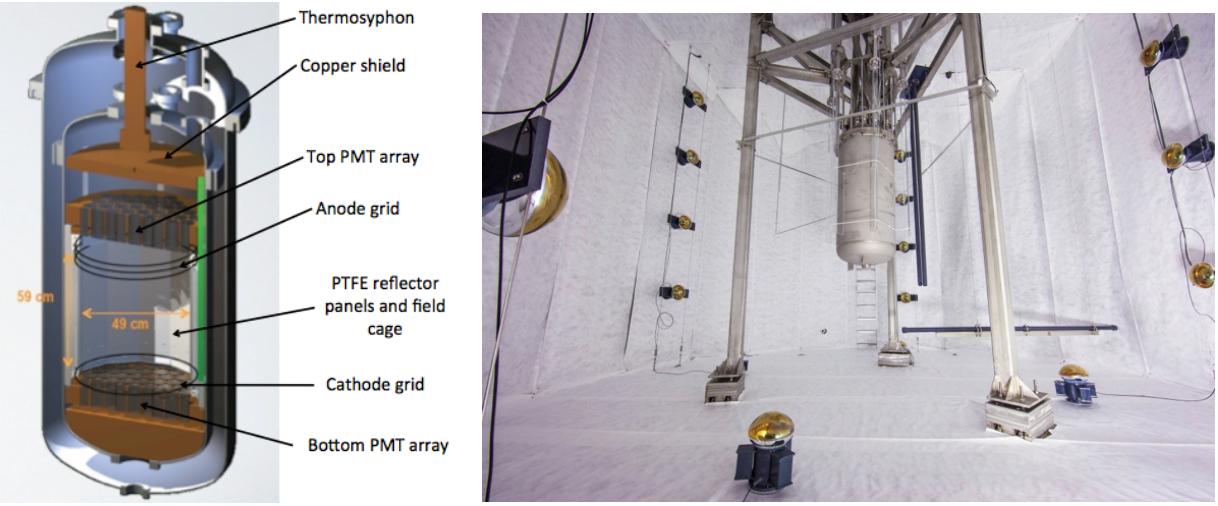

Figure 5.2.1. Left: LUX features a ~50-cm-tall, 50-cm-diameter TPC containing 250 kg of active LXe mass with PMTs at top and bottom. Right: LUX as installed in the Davis Cavern water shield.

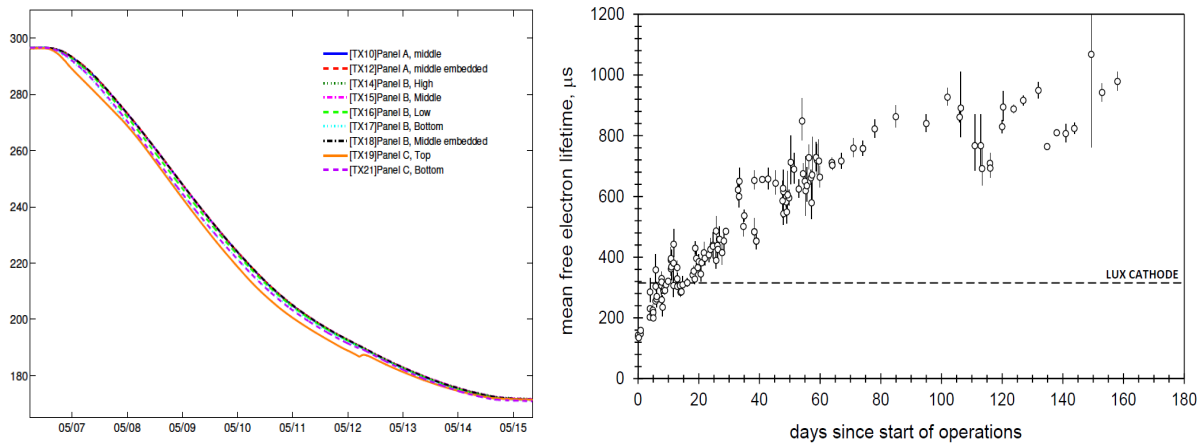

Figure 5.2.2. Left: Measured temperatures by thermometry in the polyethylene panels surrounding the active region during LUX cooldown, which was completed over a period of nine days. Right: Mean free electron lifetime, measured from the start of underground operations.

month period, during which the pressure and liquid level had sufficient stability (1% and <500 µm, respectively) to introduce no measurable variations in the S2 or S1 signals.

The 2-inch-diameter Hamamatsu R8778 PMTs used in LUX have high quantum efficiency and a low radioactive background of roughly 10 mBq/unit in terms of gamma-ray emission [38]. The low-noise amplifiers and electronics system used to read out the PMTs have resulted in ≥95% efficiency for single phe detection. The data acquisition (DAQ) system [39] features pulse-only digitization that significantly reduces the data-set size; especially important given the long drift time in LUX. The system also utilizes a sophisticated digital trigger system that will form the basis for the LZ DAQ system.

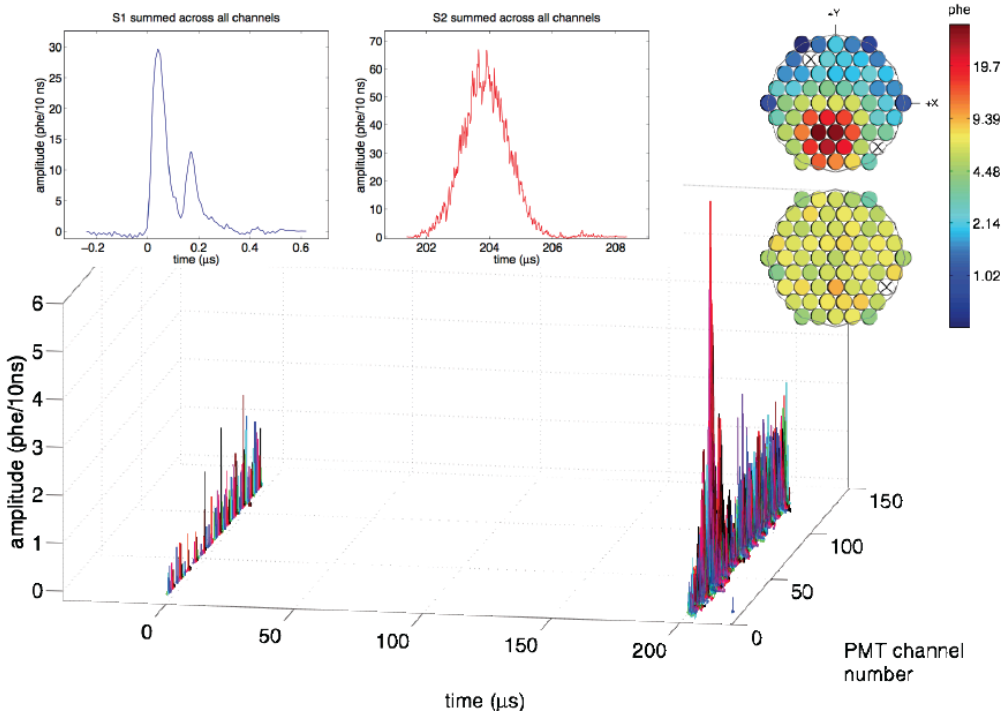

Figure 5.2.3. An example calibration event from LUX, produced from ^{83m}Kr decay.

Calibration of a large two-phase Xe TPC is difficult because of the strong self-shielding of the LXe, and the near impossibility of introducing a sealed source into the TPC interior without perturbing the fields. LUX therefore developed two novel gaseous internal calibration sources, both of which will be used for LZ. The first uses ^{83m}Kr [40], which has a ~41 keV decay and 1.8-hour half-life to stable ^{83}Kr. This was used in LUX for the first time in an extensive and ongoing way to map the position response of both S1 and S2, and the stability of these signals and other aspects of the detector, including fluid flow, electric field distribution, and electron drift length. A sample ^{83}Kr event is shown in Figure 5.2.3. The second provides a calibration of the response to the dominant background of ERs in the WIMP energy range. Here we used the beta decay of ^{3}H (18.6 keV endpoint, 12.3-year half-life), dispersed in the form of tritiated methane. The key issue is removal of this long-lived species. This was accomplished using the getter purification system, which reduced the ^{3}H concentration with a ~7-hour exponential time constant, down by at least a factor of ~10^4, at which point the ^{3}H could not be seen above other backgrounds. Finally, we have completed a novel in situ neutron calibration using mono-energetic neutrons from a DD generator deployed outside the water shield and an evacuated tube in the shield serving as a collimator.

The final backgrounds in the central fiducial region in LUX agree well with expectations based on the screening of components prior to construction, and within the WIMP region of interest was measured to be 3.6×10^{-3} events/keV/kg/day, which is the lowest ER background ever recorded below 100 keV. Background distributions within the fiducial volume are shown in Figure 5.2.4. The gamma portion is dominated by PMTs and cosmogenic activation of Cu, while the internal activity is currently dominated by ^{127}Xe (36.4-day half-life), but also has small contributions from a ^{214}Pb, a Rn daughter, and ^{85}Kr. ^{85}Kr is an especially problematic background as it is present in commercial Xe at unacceptable levels. LUX developed a chromatographic system [41] that processed 50 kg of Xe per week to an average level of 4 ppt (the initial goal was 5 ppt), with one batch doubly processed to better than a measurement limit of 0.2 ppt. Measurements at this level were made using LUX's custom mass spectrometry plus trapping technique [37].

The ER discrimination has been expected to improve with both light collection and drift field, as described in Chapter 3. Light collection was optimized in the design by maximizing surface coverage with PTFE and using high-transparency grids. The measured light-collection efficiency (phe per initial photon) of α_1=0.14 (8.4 phe/keV at 662 keV gamma rays at zero field) is the highest value yet obtained in a large LXe TPC. This high light collection has resulted in a very low S1 threshold of 4.3 keV for a 2-phe coincidence level. The drift field in LUX was limited to ~180 V/cm for stable operation in 2013. Despite this, and possibly in part due to the excellent light collection, discrimination is measured to be >99.6% using ^{3}H calibration (see Figure 5.2.5). This exceeds the original LUX goal — and in fact exceeds the LZ baseline assumption for a higher electric field. All these factors have combined to give LUX the world's best WIMP sensitivity in an initial limited duration run with a maximum sensitivity at 33 GeV/c^2 of

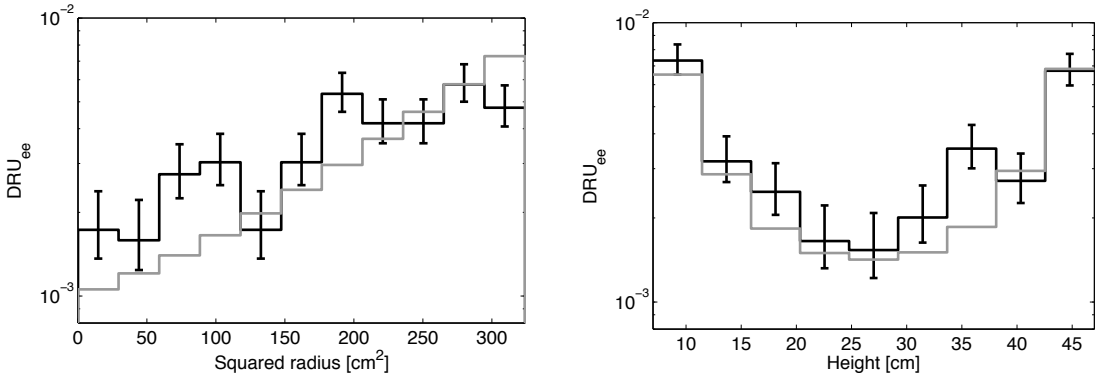

Figure 5.2.4. Low-energy measured distributions in (left) squared radius, and (right) height, within the LUX 118 kg fiducial mass, measured over the full 85.3-day WIMP search run [32]. Measured data are indicated by the black histogram with error bars. Simulation data are shown as the gray histogram.

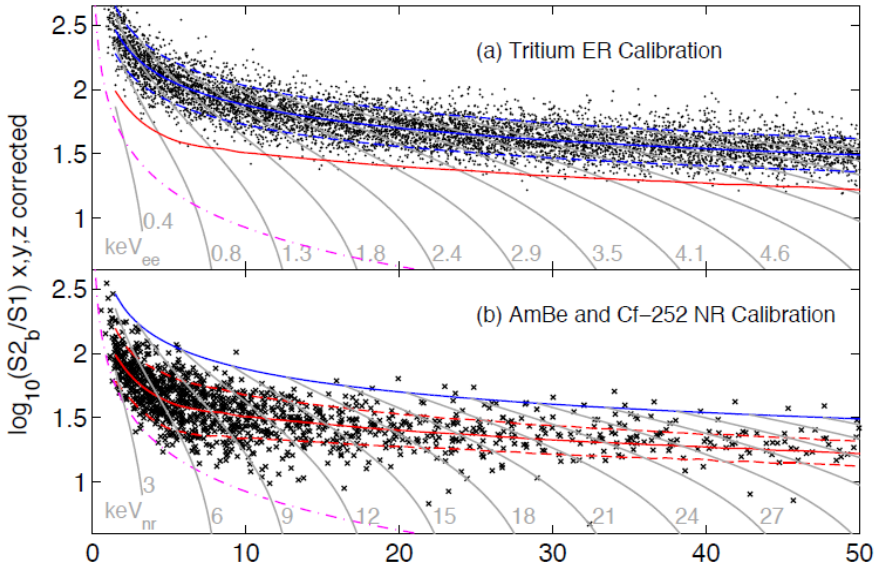

Figure 5.2.5. Discrimination demonstrated in LUX [3] with (a) ER events from beta decay of tritiated methane (discussed below) and (b) NR events from neutrons from AmBe and ^{252}Cf sources. Overlaid curves are the means and 80% inclusive bands for the ER (blue) data and NR (red) distributions. The discrimination defined by the leakage of ERs to below the NR band mean in the 2-30 pe S1 range is 99.6±0.1%. Energy contours are shown, along with (purple) the approximate location of a 200 phe cut on raw S2 size.

7.6×10^{-46} cm^2, and a powerful reach at low WIMP masses (see Chapter 1). A second, longer LUX run with improved reach started in October 2014 and is anticipated to continue into 2016.

5.3 Beyond LUX and ZEPLIN

For all the experience accumulated through the LUX and ZEPLIN programs and others, it is necessarily the case that LZ must push many aspects of this technology into new regimes in order to reach its unprecedented sensitivity. The scale-up of some subsystems is more challenging than for others, and we conclude this section with a table highlighting the key differences between LZ and LUX (Run 3) or other LXe detectors — which we indicate in brackets if not LUX. We also assign a "technical difficulty" (TD) indicator to relevant parameters, representing how significant a challenge we deem this scaling to be with respect to what has been achieved previously. We note, however, that this cannot be simply interpreted as a risk factor since we will normally have in place additional mitigation for the more challenging issues. This mitigation (e.g., R&D) is also indicated. The TD indicator ranges from "o" for minimal, to "ooo" for significant.

Table 5.3.1. Key differences between the LZ baseline design and LUX, ZEPLIN, EXO, and other experiments.

WBS Item	LZ	LUX et al.	Comments/Mitigation	TD
1: XENON				
Total mass	10,000 kg	370 kg	27x	ooo
Active mass	7,000 kg	250 kg	28x	
Fiducial mass	5,600 kg	118 kg	47x	
2: CRYOSTAT				
Material	Titanium (CP-1)	Titanium (CP-1)	Stainless steel design backup	o
U/Th activity	<0.75/0.75 mBq/kg	0.25/0.2 mBq/kg	2-year search campaign	oo
IV/OV wall	6-8/8 mm	6/6 mm		o
Max Op Pressure	4.0 bar(a)	4.0 bar(a)		o
Height	3.2 m	2 m	Excluding supports	o
Weight	1,800 kg	325 kg	Excluding supports	o
IV support	Suspended	Suspended	Fine leveling by suspension rods	oo
OV support	Bottom legs	Suspended		o
Conveyance	OV in 3 parts	Whole	Detector delivered with IV	o
3: CRYOGENICS				
Detector cooling	External delivery of subcooled LXe	Internal thermosyphons	Reduces detector complexity Allows separate system test	oo
Cooling power	1 kW	0.4 kW	Inc. Purification Tower	o
Liquid nitrogen	Cryocooler	Delivery u/g	Delivery u/g is backup	o
4: PURIFICATION				
Electron lifetime	3 ms goal 0.75 ms req.	1 ms (also Z2) (EXO >4 ms)	Emanation budget Improved gas sampling	o
Recirculation	Compressors	PTFE-diaph. pump	Higher flow, more reliable	o
Recirculation rate	500 slpm (4,300 kg/day)	25 slpm (230 kg/day)		oo
Xenon recovery	Compressor-based recovery	Cold recovery vessel + bladder	Passive capture not viable	ooo
Kr requirement	0.015 ppt	5 ppt	<0.2 ppt demonstrated	ooo
Kr sampling sensitivity	0.015 ppt	0.2 ppt	LZ sampling fully automated	oo
Radon	0.67 mBq	~10 mBq 0.4 mBq in EXO	Screening program (WBS 1.10)	ooo
5: XENON DETECTOR				
TPC length/width	1.46/1.46 m	0.5/0.5 m		o
TPC construction	Segmented rings	Vertical panels	Better electrostatics/mechanics	o
Therm. contraction	~2 cm	~0.7 cm	TPC anchored at bottom	oo
S1 Photon Det. Eff.	7%	11%	Control sources of optical extinction	ooo
Skin dielectric	4-8 cm LXe	5 cm UHMWPE	Instrumented (enhances veto)	oo

WBS Item	LZ	LUX et al.	Comments/Mitigation	TD
Cathode voltage	–100 kV (–200 kV design)	–10 kV (Z3: –10 kV)	LUX field matched at – 30 kV Extensive R&D & System Test	ooo
Cathode delivery	Own conduit	Thru skin	Risk mitigation	ooo
Rev. field region	Integral design, voltage grading	LXe gap	Better electrostatics/mechanics, Optical isolation from skin region	ooo
Field in gas	10.6 kV/cm goal	6.6 kV/cm (Z2: 8.4 kV/cm)	R&D & System Test	oo
Emission prob.	>95%	65%	Decrease delayed e-emission	oo
S2 gain	50 phe/e	14 phe/e (Z3: 30 phe/e)	Top array only	oo
PMT numbers	247/241/180	61/61/0	Top/Bottom/Skin	o
PMT model (TPC)	3-inch R11410	2-inch R8778		o
PMT activity (TPC)	3/3/30/3 mBq	10/3/66/3	^{238}U/^{232}Th/^{40}K/^{60}Co (requirements)	oo
PMT mounts	¼-inch Ti plate + trusses	Solid Cu block with cutouts	Lightweight construction Higher OD/Skin veto efficiency	o
Fluid circulation	Full sweep Min. dead space	Single in/outlet		o
TPC monitoring	Many sensors	LXe level and thermometry	HV diagnostic, protection	o
6: OUTER DETECTOR				
Vetoing media	Liquid scintillator Water Cherenkov	(Z1/2/3 vetos) Water Cherenkov	Acrylic tanks in water, common PMTs	ooo
Scintillator type	Gd-loaded LAB	(Z2 LS, Z3 plastic)	cf. Borexino, Daya Bay, SNO+	oo
Scintillator mass	27 tonnes	(Z1/2/3 ~1 tonne)		o
Scintillator purity	1.2/4.7 ppt U/Th	n/a	U at 10% Daya Bay; Th is similar	ooo
Transparency	>10 m at 430 nm	n/a		oo
Light yield	9000 ph/MeV	n/a		o
PMT channels	120	(Z2 10, Z3 52)	Using Xenon Detector DAQ	o
PMT calibration	Fibres	LEDs	Experience: SNO+, Z3	o
7: CALIBRATION				
NR calibration	AmBe, ^{252}Cf, YBe D-D generator	AmBe, ^{252}Cf D-D generator	Special YBe port and shielding	o
ER calibration (int)	^{83m}Kr, CH_3T, ^{37}Ar	^{83m}Kr, CH_3T		o
Gamma sources	Pipes in OV/IV	Pipes in water		o
8: ELECTRONICS				
Channels	1,276	122	Inc. TPCx2+Skin+OD	oo
Trigger rate	40 c/s	10 c/s	All energies	o
Pre/post-amplifiers	100	16/16	Pre- and post-amps are integrated	o
Front-end BW	30 MHz	30 MHz	At digitizer input	o
Noise	0.2 mV_{rms}	0.2 mV_{rms}	At digitizer input	o

WBS Item	LZ	LUX et al.	Comments/Mitigation	TD
Digitizers	DDC32	Struck SIS3301		o
Operating mode	POD	POD	POD: Pulse Only Digitization	o
Resolution	14 bits	14 bits	Dual range	o
Sampling	100 MS/s	100 MS/s		o
Memory depth	>163k samples for 32 channels	128k samples	~1 ms maximum drift time; For Spartan 6 FPGA; significantly larger for Kintex FPGA	o
Trigger	DDC-32	DDC-8 DSPs, Trigger Builder	LZ trigger and DAQ firmware run in parallel on the same FPGA	o
Data volume	750 TB/yr	40 TB/yr	Size of event files	o
Slow Control	MySQL custom sys + PLC system	MySQL custom sys		oo
Power	110 kW	18 kW	Maximum, full load	oo
9: ASSEMBLY & INSTALLATION				
Detector assembly	Rn-scrubbed CR, Static precautions	Surface CR, No static prec.	SURF surface building	oo
U/G deployment	Detector in IV, conv. horizontally	Detector in IV/OV + conduits, whole		ooo
10: SCREENING				
Cleanliness control	Full QA/QC	Limited QC	Control of PTFE debris	oo
HPGe screening	100 ppt, in-house	100 ppt, in-house	U/Th; already demonstrated	o
ICP-MS screening	10 ppt, in-house	Commercial	U/Th; already demonstrated	o
GD-MS screening	10 ppt, commercial	None	U/Th; already demonstrated	o
Neutron activation	20 ppt, in-house	Limited	U/Th demonstrated for PTFE	o
Rn screening	0.03 mBq, in-house	None	0.1 mBq already demonstrated	oo
Radon plate-out: wall events, (α,n)	Full QA/QC, Rn-reduced air CR,	Fiducial reduction limited Z2	QA/QC, Rn-scrubbed CR Emanation budget	ooo

Chapter 5 References

[1] G. J. Davies, W. G. Jones, J. D. Davies, J. D. Lewin, and P. F. Smith, Phys. Lett. **B320**, 395 (1994).

[2] D. B. Cline, in *Dark Matter in the Universe: Proceedings, 2nd International Symposium, February 14-16, 1996, Santa Monica, CA*, Nucl. Phys. Proc. Suppl., Vol. **51B** (1996) pp. 304–313, *On a discriminating liquid xenon detector for SUSY dark matter observation*.

[3] D. Yu. Akimov *et al.*, in *Sources and detection of dark matter and dark energy in the universe. Proceedings, 4th International Symposium, DM 2000, Marina del Rey, USA, February 23-25, 2000* (2000) pp. 461–468, *Development of a two-phase xenon discriminating detector for use in dark matter searches at the Boulby underground laboratory*, Conference Presentation.

[4] J. J. Quenby *et al.* (UK Dark Matter), Astropart. Phys. **5**, 249 (1996).

[5] B. Ahmed *et al.* (UK Dark Matter), Astropart. Phys. **19**, 691 (2003), arXiv:hep-ex/0301039 [hep-ex].

[6] G. J. Alner *et al.* (UK Dark Matter), Phys. Lett. **B616**, 17 (2005), arXiv:hep-ex/0504031 [hep-ex].

[7] G. J. Alner *et al.* (DRIFT-I), Nucl. Instrum. Meth. **A535**, 644 (2004).

[8] G. J. Alner *et al.* (DRIFT-II), Nucl. Instrum. Meth. **A555**, 173 (2005).

[9] G. J. Alner *et al.* (ZEPLIN-I), Astropart. Phys. **23**, 444 (2005).

[10] B. A. Dolgoshein, V. A. Lebedenko, and B. U. Rodionov, JETP Lett. **11**, 351 (1970).

[11] B. Edwards *et al.* (ZEPLIN-II), Astropart. Phys. **30**, 54 (2008), arXiv:0708.0768 [physics.ins-det].

[12] E. Aprile *et al.* (XENON100), J. Phys. **G41**, 035201 (2014), arXiv:1311.1088 [physics.ins-det].

[13] E. Santos *et al.* (ZEPLIN-III), J. High Energy Phys. **2011**, 115 (2011), arXiv:1110.3056 [physics.ins-det].

[14] G. J. Alner *et al.* (ZEPLIN-II), Astropart. Phys. **28**, 287 (2007), arXiv:astro-ph/0701858 [astro-ph].

[15] G. J. Alner *et al.* (ZEPLIN-II), Phys. Lett. **B653**, 161 (2007), arXiv:0708.1883 [astro-ph].

[16] D. Yu. Akimov *et al.* (ZEPLIN-III), Astropart. Phys. **27**, 46 (2007), arXiv:astro-ph/0605500 [astro-ph].

[17] V. N. Lebedenko *et al.* (ZEPLIN-III), Phys. Rev. **D80**, 052010 (2009), arXiv:0812.1150 [astro-ph].

[18] V. N. Lebedenko *et al.* (ZEPLIN-III), Phys. Rev. Lett. **103**, 151302 (2009), arXiv:0901.4348 [hep-ex].

[19] D. Yu. Akimov *et al.* (ZEPLIN-III), Phys. Lett. **B709**, 14 (2012), arXiv:1110.4769 [astro-ph].

[20] V. Chepel and H. Araújo, J. Instrum. **8**, R04001 (2013), arXiv:1207.2292 [physics.ins-det].

[21] D. Yu. Akimov *et al.* (ZEPLIN-III), Astropart. Phys. **34**, 151 (2010), arXiv:1004.4207 [hep-ex].

[22] P. Majewski *et al.* (ZEPLIN-III), in *Position sensitive detectors. Proceedings, 9th International Conference, PSD9, Aberystwyth, UK, September 12-16, 2011*, J. Instrum. **7**, C03044 (2012), arXiv:1112.0080 [physics.ins-det].

[23] H. M. Araújo *et al.*, Nucl. Instrum. Meth. **A521**, 407 (2004).

[24] H. M. Araújo *et al.* (ZEPLIN-III), Astropart. Phys. **35**, 495 (2012), arXiv:1104.3538 [physics.ins-det].

[25] C. Ghag *et al.* (ZEPLIN-III), Astropart. Phys. **35**, 76 (2011), arXiv:1103.0393 [astro-ph].

[26] L. Reichhart *et al.* (ZEPLIN-III), Astropart. Phys. **47**, 67 (2013), arXiv:1302.4275 [physics.ins-det].

[27] V. N. Solovov *et al.* (ZEPLIN-III), in *Nuclear Science Symposium and Medical Imaging Conference (NSS/MIC), 2011 IEEE* (2011) pp. 1226–1233, *Position Reconstruction in a Dual Phase Xenon Scintillation Detector*; V. N. Solovov *et al.* (ZEPLIN-III), IEEE Trans. Nucl. Sci. **59**, 3286 (2012), arXiv:1112.1481 [physics.ins-det].

[28] F. Neves *et al.* (ZEPLIN-III), J. Instrum. **6**, P11004 (2011), arXiv:1106.0808 [astro-ph].

[29] F. Neves *et al.* (ZEPLIN-III), Astropart. Phys. **33**, 13 (2010), arXiv:0905.2523 [physics.ins-det].

[30] M. Horn *et al.* (ZEPLIN-III), Phys. Lett. **B705**, 471 (2011), arXiv:1106.0694 [physics.ins-det].

[31] D. S. Akerib *et al.* (LUX), Nucl. Instrum. Meth. **A704**, 111 (2013), arXiv:1211.3788 [physics.ins-det].

[32] D. S. Akerib *et al.* (LUX), Phys. Rev. Lett. **112**, 091303 (2014), arXiv:1310.8214 [astro-ph].

[33] D. S. Akerib *et al.* (LUX), "Radio-assay of Titanium samples for the LUX Experiment," (2011), arXiv:1112.1376 [physics.ins-det].

[34] D. S. Akerib *et al.* (LUX), Astropart. Phys. **45**, 34 (2013), arXiv:1210.4569 [astro-ph].

[35] D. S. Akerib *et al.* (LUX), Nucl. Instrum. Meth. **A709**, 29 (2013), arXiv:1207.3665 [physics.ins-det].

[36] D. S. Leonard, A. Dobi, C. Hall, L. Kaufman, T. Langford, S. Slutsky, and Y.-R. Yen, Nucl. Instrum. Meth. **A621**, 678 (2010), arXiv:1002.2742 [physics.ins-det].

[37] A. Dobi, C. G. Davis, C. Hall, T. Langford, S. Slutsky, and Y.-R. Yen, Nucl. Instrum. Meth. **A665**, 1 (2011), arXiv:1103.2714 [astro-ph].

[38] D. S. Akerib *et al.* (LUX), Nucl. Instrum. Meth. **A703**, 1 (2013), arXiv:1205.2272 [physics.ins-det].

[39] D. S. Akerib *et al.*, Nucl. Instrum. Meth. **A668**, 1 (2012), arXiv:1108.1836 [astro-ph].

[40] L. W. Kastens, S. B. Cahn, A. Manzur, and D. N. McKinsey, Phys. Rev. **C80**, 045809 (2009), arXiv:0905.1766 [physics.ins-det].

[41] A. I. Bolozdynya, P. P. Brusov, T. Shutt, C. E. Dahl, and J. Kwong, in *Proceedings of the 11th Symposium on Radiation Measurements and Applications Ann Arbor, MI, USA 23–26 May 2006*, Nucl. Instrum. Meth., Vol. **A579** (2007) pp. 50–53, *A chromatographic system for removal of radioactive ^{85}Kr from xenon*.